ACS OMEGA

http://pubs.acs.org/journal/acsodf

Article

Using Asphalt as an Additive for Waste Cross-Linked Polyethylene Recycled Materials to Improve Thermoplastic Processing

Yi Liao, Shuangxin Lai, Shuangqiao Yang, Jinjing Liu, Adrian L. Kelly, and Shibing Bai*

Cite This: *ACS Omega* 2022, 7, 19113−19121

Read Online

ACCESS | Metrics & More | Article Recommendations

ABSTRACT: With good insulation, cross-linked polyethylene (XLPE) cables are widely used as an important basic material for power transportation. Due to being insoluble and infused, the cross-linked network structure caused a challenge in the recycling of waste XLPE, which is usually treated by incineration and landfilling. In this research, XLPE was part-de-cross-linked via solid-state shear milling (S^3M) technology, but the resulting powder was difficult to process. In order to improve the re-processability of XLPE, asphalt with a similar structure was added during the thermoplastic processing. To deeply understand the influence of asphalt on the matrix, the compatibility, dispersion, and rheological properties of the composites were characterized. Due to the good compatibility between de-cross-linked XLPE and asphalt, the viscosity of the composites decreased significantly. Some sea-island structures also formed in composites, which increased the toughness of the composites, so the elongation at break reached as high as 322%. The use of asphalt to achieve the processing performance of part-de-cross-linked XLPE powder was highly effective. Furthermore, the prepared composites showed potential application in the field of waterproofing, which could recycle waste XLPE cables on a large scale.

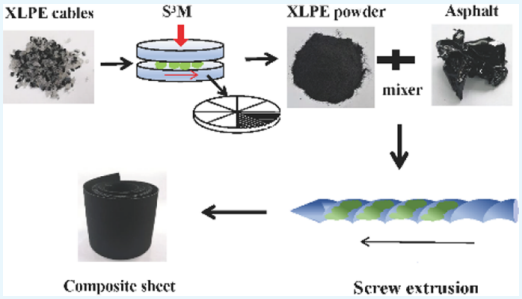

1. INTRODUCTION

Cross-linked polyethylene (XLPE) as a kind of thermoset plastic with a three-dimensional network structure[1] has good mechanical properties, heat resistance, environmental stress cracking resistance, and chemical resistance. The above variety of characteristics enable XLPE to be widely used in pipes, cables, and other fields.[2,3] Yearly, a large number of waste XLPE cables cannot be recycled efficiently and cheaply.[4−6] The recycling of thermoset plastics solves the environmental pollution caused by landfills and incineration and avoids waste of oil resources.[7] It is a huge challenge to achieve green, efficient recycling of XLPE.[8]

According to the literature, there are many methods for recycling waste XLPE,[9] including thermal shear plasticization recycling,[10,11] powdered filler recycling, supercritical fluid recycling, and ultrasonic-assisted recycling,[12−14] which have disadvantages of poor mechanical properties of materials, large equipment investment, and strict process requirements.[15−17] In order to recycle XLPE in a simple and efficient way, solid-state shear milling (S^3M) technology was used.[18−20] S^3M equipment is based on a traditional Chinese stone pan mill, which is a mechanochemical reactor. With the unique three-dimensional shear structure, the materials in the equipment are subjected to shearing, squeezing, and stretching stress fields.[21] The motion trajectory of materials is a spiral line, increasing the milling path, which can realize the functions of crushing, dispersing, mixing, etc.[21] It can be applied to destroy the cross-linked bond of silane cross-linked polyethylene (Si-XLPE) and achieve the fracture between some −C−Si− and −O−Si−O− bonds,[20] resulting in the thermoplastic processing of Si-XLPE. However, different from the heterogeneous cross-link network of Si-XLPE, the cross-linked bond of P-XLPE is the same as the C−C chemical bond of the main chain, so it belongs to a homogeneous network structure.[22] When P-XLPE is treated with S^3M technology, the mechanochemistry is random and non-selective. The main polymer chain and cross-linking bond are randomly fractured, resulting in the fluidity of powder processing being strengthened. This limits the use of recycled materials, which are mostly used as an additive to modify asphalt.[20,23] Large-scale recycling of discarded P-XLPE is still a serious problem.

Asphalt is the residue of coking or crude oil distillation, and it is mainly composed of alkane compounds composed of carbon and hydrogen.[24] Due to its waterproof, moisture-proof, and corrosion-proof characteristics, asphalt is often used in the field of waterproofing and paving roads. The well-known Pitch drop experiment shows that asphalt can flow even at room temperature. Asphalt can flow easily at a certain temperature

Received: December 2, 2021
Accepted: March 2, 2022
Published: May 28, 2022

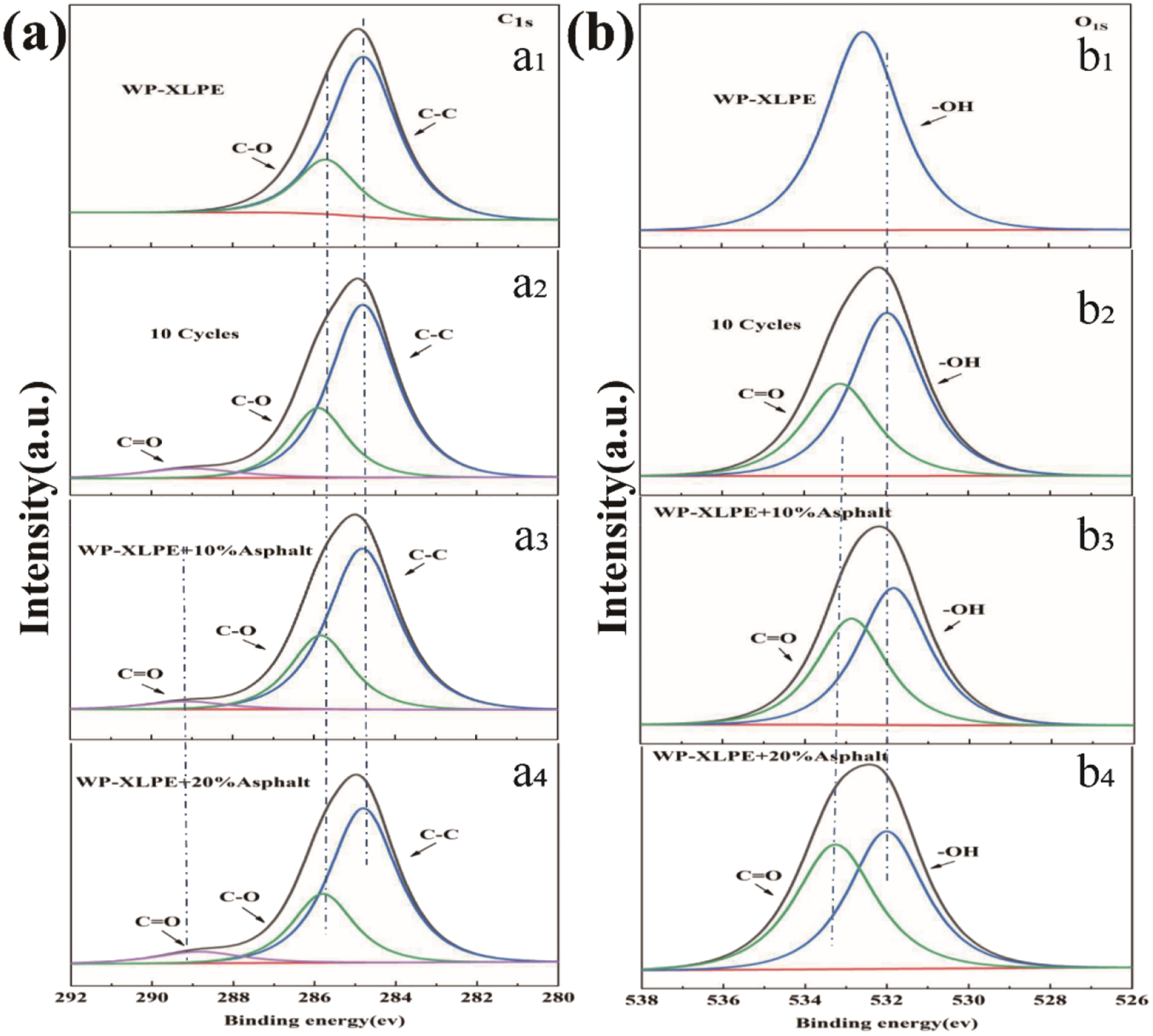

Figure 1. Comparison of XPS spectra of WP-XLPE without treatment and after milling for 10 cycles: XPS spectra for C_{1s} (a_1, a_2) and O_{1s} (b_1, b_2). Comparison of XPS spectra of the composites with different asphalt contents: XPS spectra for C_{1s} (a_3, a_4) and O_{1s} (b_3, b_4).

and is compatible with P-XLPE so that the improvement of P-XLPE powder thermoplastic processing can be realized. Recently, we proved the feasibility of the use of de-cross-linked P-XLPE in asphalt-based waterproof materials.[25] However, asphalt-based waterproof materials cannot be used at temperatures above 50 °C, which limited the application of waterproof materials. The addition of asphalt into polymer-based waterproof materials offers potential solutions to this challenge.

This study provides the novel application of asphalt in waste peroxide cross-linked polyethylene (WP-XLPE) composite. Firstly, S^3M technology was used to deal with WP-XLPE cables, which are composed of more than 75% P-XLPE and about 25% EVA. Through the strong shear stress of S^3M equipment, the cross-linking network was damaged to a certain extent, and WP-XLPE powder was obtained. Then, asphalt was added to the WP-XLPE matrix as an additive to improve the processing performance. The result showed that the asphalt and WP-XLPE had good compatibility and uniform dispersion. Also, the addition of asphalt greatly improved the thermoplastic processing capacity of WP-XLPE. The composite sheets can be successfully obtained by extrusion processing, which has the potential to be used as a waterproof material.

2. RESULTS AND DISCUSSION

2.1. Changes in Chemical Bonds and Groups of Materials. X-ray photoelectron spectroscopy can obtain chemical bond composition information in the range of 2−10 nm on the surface of the material. The XPS spectrum of the WP-XLPE cable before and after milling is in Figure 1. In the high-resolution spectra of C and O, it can be seen that the powder after milling has a new peak at the position corresponding to the carbonyl group,[26] indicating that when the powder is decomposed by force, there is indeed a process of reacting with oxygen to form a C═O bond. This is a part of the methylene groups deformed and broken under the action

https://doi.org/10.1021/acsomega.1c06825
ACS Omega 2022, 7, 19113−19121

of considerable mechanical stresses by S^3M technology and oxidized into new carbonyl groups.[27−31] The presence of the carbonyl group enhances the polarity of WP-XLPE and contributes to a stronger intermolecular force between the matrix and asphalt.[32] However, the EVA in the cable brings natural hydroxyl groups to the WP-XLPE powder, which can also be seen in the results.[33] This shows that the S^3D equipment developed by our research group is not simply a grinding process but a solid-phase mechanochemical reactor. In this process, the thermosetting cross-linked molecular structure is destroyed, and the chemical bonds are partially reorganized.

Figure 1 also shows the C and O high-resolution spectra of asphalt-modified WP-XLPE composites with different contents. Compared with the pure WP-XLPE without asphalt, the content of the C═O bond has increased from 39.8 to 51%, which indicates that the free radicals generated during the milling process are continuously oxidized to produce carbonyl groups during the thermoplastic processing. Since there was no chemical bond breaking or formation during the asphalt modification process, no new peaks appeared in the XPS results. The above results indicate that physical melting is the main process in the modification of P-XLPE.

2.2. Distribution of Asphalt and WP-XLPE. To carefully observe the phase morphology of the two-phase distribution, the cross section of the composite material was analyzed by SEM. As shown in Figure 2, the section of the pure XLPE

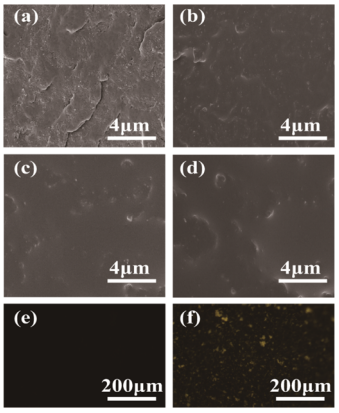

Figure 2. SEM images of the fracture surface of WP-XLPE/asphalt composites: without asphalt (a), 10 wt % asphalt (b), 20 wt % asphalt (c), and 30 wt % asphalt (d). Fluorescence microscope micrographs of pure XLPE (e) and composite with 20 wt % asphalt (f).

without asphalt is not only randomly scattered with particles but also has many scaly protrusions; on the contrary, the section of the composite with asphalt is very flat, with no trace of fillers at all. It can be concluded that the two-phase dispersion is very uniform, and there is no phase separation or incompatibility. Actually, WP-XLPE cables are a complex mixture, in which the inorganic filler hinders the flow of the melt during the melting process. The section without asphalt shows that the distribution of these fillers is very uneven, which affects the performance of the material. The addition of asphalt wraps these fillers and makes the fillers more smoothly distributed in the matrix. Even in the cross section, their existence cannot be seen, showing a very smooth shape. Fluorescence microscopy is an effective technique for observing the microstructure of asphalt.[38,39] As shown in Figure 2e,f, pure XLPE did not show a fluorescence phenomenon; on the contrary, composite materials with asphalt showed a uniform fluorescence phenomenon. This further indicates that asphalt is well dispersed in the XLPE matrix.

Observing the etched section in Figure 3, it is seen that there are circular or deep groove-like voids left by the asphalt after

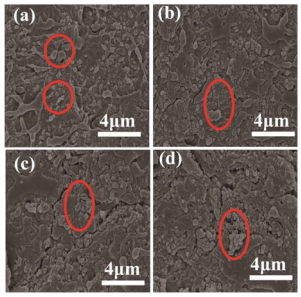

Figure 3. SEM images of the fracture surface after etching of WP-XLPE/asphalt composites: 10 wt % asphalt (a), 20 wt % asphalt (b), 30 wt % asphalt (c), and 40 wt % asphalt (d).

being etched, which shows that the asphalt has a dispersed state and a continuous state. The protruding part of the red circle shows the insoluble cross-linked sections forming island structures. The distribution between asphalt and WP-XLPE has both a typical island-like structure surrounded by asphalt and a sheet-like structure after melting, indicating that the 3D network structure is destroyed under the action of solid-state mechanochemistry.[40]

Under the effect of S^3M technology, WP-XLPE is divided into two parts: fusible polyethylene and a non-melting cross-linked network. It brings about two different behaviors under interaction with asphalt: the movable part of the chain formed under shear is melted and mixed with asphalt to form an interlocking continuous layered structure because of the similar chemical composition and structure and the infusible part is wrapped in asphalt to form an island structure.

Based on all the discussions above, the schematic diagram of the mutual distribution relationship among asphalt, the cross-linking section, and the de-cross-linking section is drawn in Figure 4. This figure intuitively reflects that in the ternary

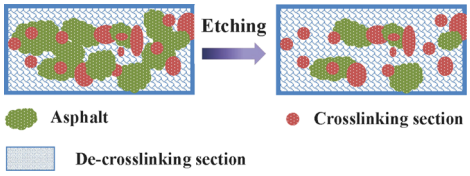

Figure 4. Diagram of the distribution of three components in a composite.

blending system, asphalt is compatible in the continuous phase of the fusible de-cross-linking section, while the cross-linked section becomes the dispersed phase. Apparently, the asphalt interacts with the fusible section, and a small amount of asphalt is dissolved into the cross-linking particle. Asphalt, a complex additive, is connected to three parts, namely, amorphous, crystalline, and cross-linked. It moves the molecular chain more smoothly at high temperatures and more regularly during thermoplastic processing. In addition, the sea-island structure provides toughness to the material.

https://doi.org/10.1021/acsomega.1c06825
ACS Omega 2022, 7, 19113−19121

2.3. Compatibility of Asphalt and WP-XLPE. To explore the molecular chain changes of waste XLPE treated with S^{3}M, low-field nuclear magnetic resonance (LF-NMR) relaxation properties were used to study the molecular motility, and the following results were obtained. As shown in Figure 5a,

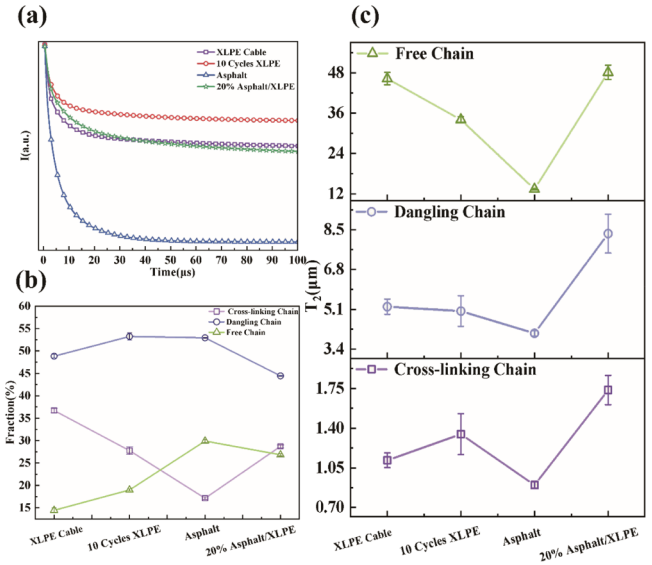

Figure 5. Variation of signal attenuation with time in low-field nuclear magnetic resonance (LF-NMR) tests (a). Fractions of cross-linking chains, dangling chains, and free chains in unmilled and milled for 10 cycles of asphalt and 20% asphalt /XLPE composites (b) and respective T_2 (c).

the signal intensity of an unmilled XLPE cable material attenuates to equilibrium faster than that of milled powder, which is because the action of S^{3}M brings the opportunity of easier movement to the powder. The composites with attenuation rates between these two indicate that there is a certain interaction between asphalt and the XLPE matrix. As shown in Figure 5b, the fraction of free chains and dangling chains increased after milling, while the content of cross-linked chains decreased significantly. The T_2 corresponding to the three molecular chains is shown in Figure 5c. The slower the molecule moves, the smaller the size and the closer the bond is, resulting in the smaller T_2.[34] Compared with before and after S^{3}M treatment, it can be seen that the cross-linked section moves easily and its structure is loose after a high shear action.[35] It is worth mentioning that the T_2 of the three molecular chains of asphalt /XLPE composites increased significantly, confirming that asphalt as an additive did improve the thermoplastic processing of the XLPE matrix. In summary, S3M technology can destroy part of the XLPE cross-linking structures, which means that some C−C bonds do not have a selective fracture.

The dynamic mechanical properties are shown in Figure 6. The result of DMA reflects the good compatibility of asphalt and WP-XLPE. The α and β transition peaks of different asphalt contents are in the same temperature range, indicating that the compatibility between the two phases is good; in other words, the addition of asphalt does not affect the tan δ of WP-XLPE. The transition area of adding asphalt becomes narrower, which also shows that the distribution between the two phases is uniform.[36] The increase in peak intensity, mainly contributed by the amorphous phase, is due to the easier movement of small molecules in the asphalt component, which makes the segment movement more frictional.[37] The movement of the relaxation temperature to high temperatures indicates that the amorphous WP-XLPE is arranged more regularly under the action of asphalt, and the structure density is improved, which makes up for the disordered structure caused by the solid-phase mechanochemistry. Combined with the LF-NMR results that the overall relaxation signal attenuation rate of the composites is faster than that of XLPE without asphalt, it can be concluded that asphalt does interact with the easily moving part of the XLPE matrix to a certain extent.

The storage modulus reflects the rigidity of the material. As shown in Figure 6b, the content of asphalt has a significant effect on it. When the temperature is below zero, the chain segment is frozen and yet to move, but the lower-molecular-weight asphalt can better transfer the force received to the rigid particles, thereby increasing the storage modulus of the material. In addition, as the temperature increases, the matrix begins to soften, and with relaxation, the storage modulus decreases. Contrary to the elastic modulus, the loss modulus is a measure of the energy loss when the composite material is deformed to reflect the toughness of the material. The loss modulus peak around −25 °C in the Figure 6c indicates that the asphalt makes the amorphous part of WP-XLPE more regular and hinders the movement of the chain segment. There is a rule that the higher the content, the more obvious the restriction.

2.4. Thermal Performance. As shown in Figure 7a,b, with the addition of asphalt, the processing temperature of the material is significantly reduced. There is also a trend that the

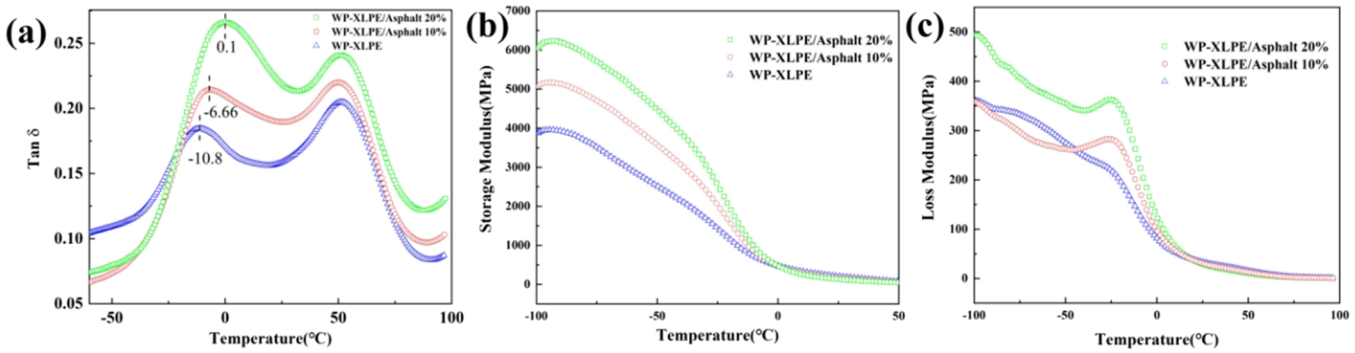

Figure 6. DMA curves of WP-XLPE/asphalt composites with different asphalt contents. Loss angle tan δ curves (a); storage modulus curves (b); and loss modulus curves (c).

https://doi.org/10.1021/acsomega.1c06825
ACS Omega 2022, 7, 19113−19121

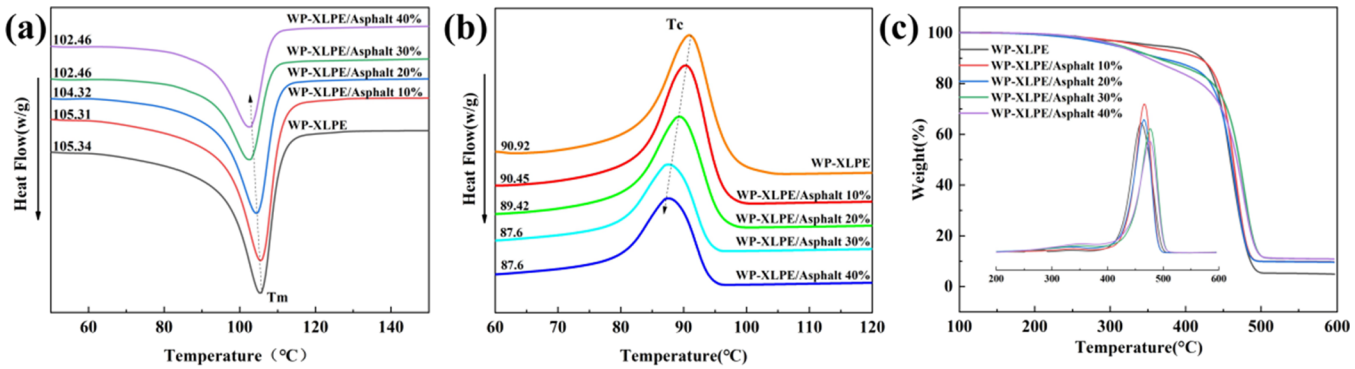

Figure 7. DSC heating curves of composites with different asphalt contents (a). DSC cooling curves of composites with different asphalt contents (b). TGA curves of composites with different asphalt contents (c).

higher the amount added, the more obvious the melting temperature and crystallinity will decrease. According to the results shown in Figure 7a, the crystallinity (Xc) of materials with different asphalt additions can be calculated. There is no doubt that the addition of asphalt reduces the crystallinity because of the interaction between asphalt and polyethylene molecules, which impedes the crystallization process. The content of asphalt destroys the crystal lattice arrangement of PE and affects the crystallization process of its material, causing the formation of an imperfect crystal, resulting in a decrease in melting temperature and crystallinity[41] (Table 1).

Table 1. Crystallinity of Composites with Different Asphalt Contents

Sample	Crystallinity of Composites				
asphalt content (%)	0	10	20	30	40
Xc (%)	20	18.97	15.96	13.27	10.82

During the cooling crystallization process, the endothermic peak shifts to low temperatures with the addition of asphalt. The reason is that the volume of molecular chain movement increases so that crystallization can be achieved at lower temperatures.[42] In addition, this also reflects that the addition of asphalt makes the molecular chain move easily and contributes to good thermoplastic processing performance.

As far as the thermal stability in Figure 7c is concerned, the thermal weight loss of materials mainly includes two stages: the first stage is 250−400 °C, which is mainly the thermal degradation of EVA and asphalt and the second stage is 400−500 °C, which is mainly the thermal degradation of the WP-XLPE matrix. Obviously, the whole process is mainly based on the second stage. In the first stage, because asphalt is a low-molecular-weight mixture with an average molecular weight of about 1000, as the temperature increases, the asphalt in the composite material begins to decompose first. The low-temperature decomposition is relatively stable, but the mass loss at this temperature increases with the increase in the asphalt content. In the second stage, the decomposition temperature tends to move to high temperatures with the addition of asphalt, indicating that the thermal stability of the composite material has become better.[43]

2.5. Processing Performance. In this paper, a high-pressure capillary rheometer was used to test the processing performance of composite materials with different asphalt additions. It can be seen from Figure 8a that this is a typical shear thinning situation, and as the asphalt content increases, the shear viscosity of the material decreases, especially in the low-frequency range.[44] The same result can also be obtained in the torque rheology curve in Figure 8b. When the asphalt addition amount is 20%, the torque drops suddenly, indicating that the melt viscosity is low and the thermoplastic processing is easier. This shows that when the material is in the molten state, asphalt as a modifier moves between the cross-linked phase and the amorphous phase.[45] At the same time, it plays a role in reducing the entanglement and friction between the molten phase and the infused phase to make the melt flow smoothly. This also macroscopically confirmed the LF-NMR results. Microscopically, under the influence of asphalt, the cross-linking, dangling, and free molecular chains of the composites all have larger relaxation times, indicating that the whole molecular chain is easier to move. Macroscopically, the

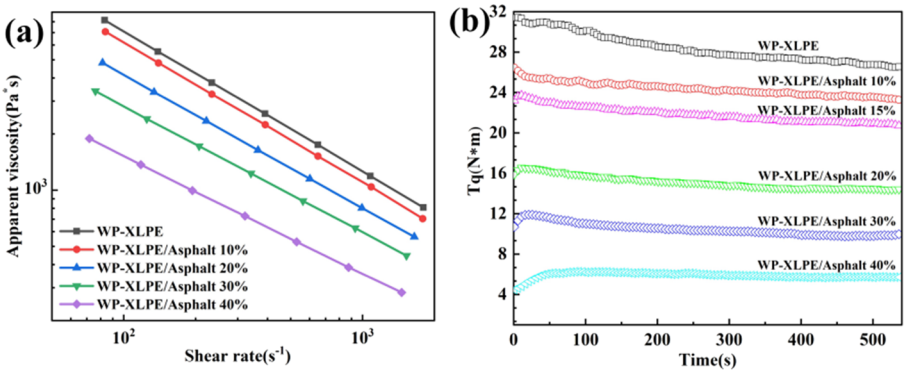

Figure 8. Capillary rheological curve (a) and the torque variation (b) of composites with different asphalt contents.

https://doi.org/10.1021/acsomega.1c06825
ACS Omega 2022, 7, 19113−19121

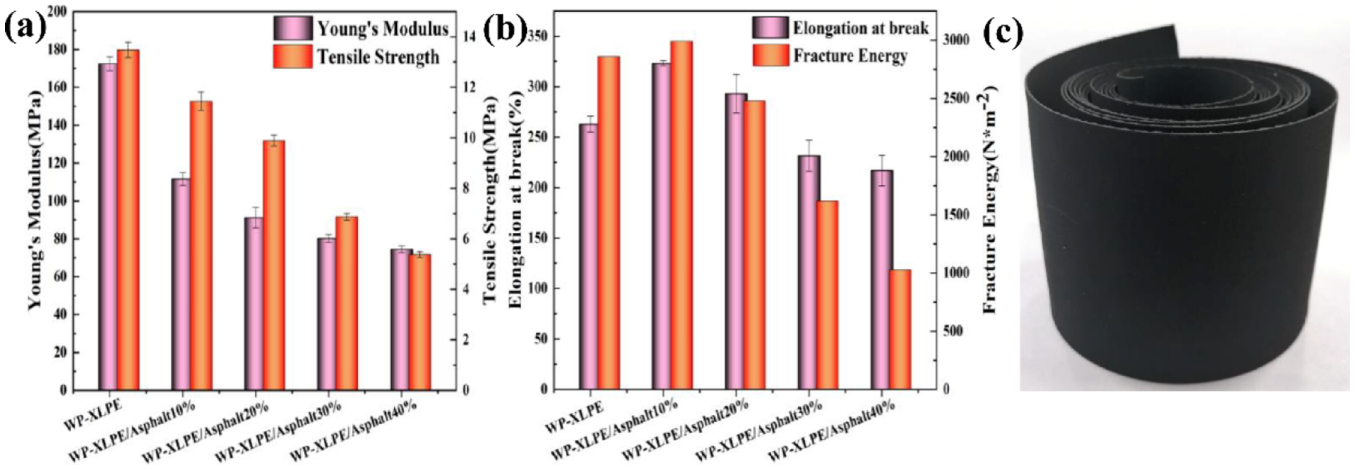

Figure 9. Tensile performance of composites with different asphalt contents (a, b). Digital photographs of WP-XLPE/asphalt extruded sheet blends (c).

thermoplastic fluidity of composite materials is enhanced and the processability is improved. In addition, it also reflects that the addition of asphalt can indeed improve the thermoplastic properties of the matrix. The fusible sections of the composite are interspersed with each other, and the good fluidity of asphalt brings low viscosity to the cross-linked parts. The volume effect is caused by the small molecular components of asphalt because of the addition increasing the distance between polymer molecules and decreasing the force between the molecules.[46,47] The weakening of van der Waals force brings about a drop in melt viscosity. The existence of asphalt makes up for the shortcomings of the difficult thermoplastic processing of pure WP-XLPE powder. In addition, the fusible parts of the composite are interspersed with each other, and the good fluidity of asphalt brings low viscosity to the cross-linked parts. In a word, the addition of asphalt can indeed improve the thermoplastic properties of the matrix.

2.6. Mechanical Performance. The tensile data of pure WP-XLPE in Figure 9 shows that after 10 times milling, the waste cable material has regained the thermoplastic processability and the recycled material also has a better mechanical performance. This is consistent with the statement in a large number of documents: S^3M technology has the function of de-cross-linking and provides ideas for recycling thermoset plastics. For asphalt-modified WP-XLPE composite materials, the addition of asphalt not only improves the processing performance of WP-XLPE but also affects the mechanical properties of the material. As the asphalt content increases, Young's modulus and tensile strength decrease to a certain extent, but the fracture energy and elongation at break have a peak. When the asphalt content is 10%, the elongation can reach 322%, and the tensile strength remains above 10 MPa. The reasons for the above phenomenon are as follows: asphalt has the effect of weakening the intermolecular force of WP-XLPE, increasing the fluidity of the molecular chain, and reducing the crystallinity of the molecular chain, which leads to a decrease in strength and an increase in toughness. Finally, it can be directly processed by screw extrusion to obtain a sheet with a stable structure and smooth surface, as shown in Figure 9c.

3. CONCLUSIONS

WP-XLPE powder with thermoplastic processing properties can be prepared by S3M technology. However, the filler and cross-linking section of a cable hinder the movement of molecular chains, which is not conducive to the reprocessing of recycled materials. Without stable flow and smooth surface, the material cannot be extruded by screw. The purpose of this study is to improve the melt fluidity of WP-XLPE. The addition of asphalt could solve the dispersion relationship among the filler, cross-linked part, and de-cross-linked part. Due to the principle of "like dissolves like", the two have good compatibility. Furthermore, the role of asphalt is also highlighted, increasing the intermolecular gap, promoting molecular movement, and reducing melt viscosity, which effectively reduced the difficulty of thermoplastic processing. The asphalt with good fluidity also entrains the filler in WP-XLPE to make it more evenly dispersed in the matrix. In addition, the asphalt and the non-melting cross-linked part form a sea-island structure, which enhances the toughness of the material to a certain extent. When the asphalt content is 10%, the elongation can reach 322%, and the tensile strength remains above 10 MPa. Different from the complex process of traditional waterproofing membranes, this material can be directly prepared into continuous membranes by screw extrusion. At last, the use of a WP-XLPE cable material as the matrix also provides a new direction for large-scale recycling of waste, bringing considerable economic and social benefits.

4. MATERIALS AND METHODS

4.1. Materials. The waste peroxide cross-linked polyethylene cable mainly includes three parts, a conductor shielding layer, insulating layer, and insulating shielding layer, provided by TBEA Deyang Cable Co., Ltd. (Sichuan China), which was consisted of 75% P-XLPE and 25% EVA.

For the 90# asphalt, the label is determined by the penetration degree, and its basic performance is shown in Table 2, provided by Beijing Oriental Yuhong Co., Ltd.

4.2. Preparation of Asphalt/WP-XLPE Composites. The preparation scheme of asphalt/WP-XLPE composites is shown in Figure 10. The WP-XLPE cable was crushed into 2−3 cm particles by a plastic crusher and then fed into the solid-state shear milling (S^3M) equipment to prepare the WP-XLPE

https://doi.org/10.1021/acsomega.1c06825
ACS Omega 2022, 7, 19113−19121

Table 2. Basic Properties of Asphalt

asphalt	90
needle penetration/25 °C (0.1 mm)	80−90
ductility/10 °C (cm)	>20
softening point (°C)	42−49
wax content (%)	<2.6
solubility in trichloroethylene (%)	>99.9

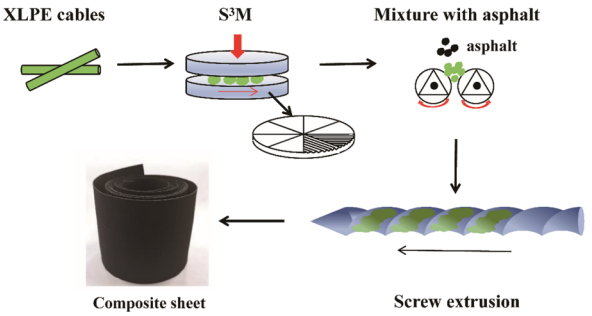

Figure 10. Scheme of recycling WP-XLPE and preparing composite sheet.

powder with 10 milling cycles at 50 rpm. In this milling process, the temperature is controlled by the cooling water. The instrument mainly consisted of two milling pans with a lot of grooves and ridges. The huge shear force resulted from the relative motion between the two pans. At the same time, the material spiraled outward from the center of the pan at a rotation speed.

The WP-XLPE powder was mixed with asphalt of different mass ratios through an internal mixer at a speed of 50 rpm and under a temperature of 180 °C. Ten minutes later, the material was taken out and crushed. Then, the composite material fragments were made into sheets in two ways: the first one, under 180 °C and 10 MPa, hot pressing for 10 min, then cold pressing under the same pressure for 10 min; the second one, extruding with a screw extruder, with the screw speed being maintained at 100 rpm. It is worth mentioning that the temperature was set to 150, 175, and 180 °C successively from the feeding section, and the die temperature was 175 °C.

4.3. Characterization. *4.3.1. X-ray Photoelectron Spectroscopy (XPS).* An X-ray photoelectron spectrometer, which is a Kratos Nova instrument equipped with a monochromatic Al kαX-Ray source ($h\upsilon$ = 1486.6 eV), was used to identify all the elements present in the composite material through an accelerating voltage of 15 kV and an emission current of 10 mA.

4.3.2. Low-Field Nuclear Magnetic Resonance (LF-NMR). The restricted molecular motion was recorded on a VTMR20-010V-T low-field spectrometer (NIUMAG, China) at 20 MHz proton resonance frequency. The experimental temperature was controlled at 125 ± 0.01 °C. The magic-sandwich echo (MSE) sequence was used to avoid the loss of the rapidly decaying rigid-phase signals in the free induction decay (FID) caused by the dead time of the receiver. A Carr−Purcell−Meiboom−Gill (CPMG) sequence was used to eliminate magnetic field inhomogeneity and refocus the chemical shift anisotropy. Consequently, the combination of the MSE−FID sequence at a short acquisition time (~80 μs) and CPMG sequence at a long echo time (80−106 μs) was used to obtain a fully recovered FID. The $\pi/2$ and π pulse lengths in the CPMG sequence were 3.0 μs and 5.28 μs, respectively.

4.3.3. Dynamic Mechanical Analysis (DMA). A DMA from TA Instruments (model Q850) in three-point bending mode was utilized to study the dynamic mechanical properties of specimens. Dynamic loss (tan δ) was determined at a frequency of 1 Hz and a heating rate of 3 °C·min^{-1}as a function of temperature in the range of −100 to 100 °C.

4.3.4. Scanning Electron Microscopy (SEM). All asphalt/WP-XLPE composites of different components were brittle fractured in liquid nitrogen and then immersed in *n*-hexane to etch away the asphalt. The morphology of the cross-section was observed with an Inspect (FEI) scanning electron microscopy instrument to analyze the polymer morphology and the distribution of asphalt in the matrix. All samples were sputter-coated with gold.

4.3.5. Fluorescence Microscopy. The distribution and phase morphology of asphalt in composites were observed by a Nikon 80i fluorescence microscope (Japan). The laminated composite was placed on a glass slide and viewed with green excitation light from a fluorescence microscope.

4.3.6. Differential Scanning Calorimetry (DSC). A TA Q20 differential scanning calorimeter was used to test the melting and crystallization behavior of composite samples, with nitrogen atmosphere protection to prevent the change in asphalt composition. The DSC curve was recorded, with a temperature range of −70 to 200 °C, at a heating rate of 10 °C·min^{-1}. In this temperature range, the sample underwent a process from heating to cooling. The crystallinity (Xc) of polyethylene in the composite was calculated, where the standard melting enthalpy was 290 J/g.[48]

4.3.7. Thermogravimetric Analysis (TGA). A TGA-Q50 from TA Instruments was used to study the thermal stability of composite asphalt materials using a heating rate of 10 °C·min^{-1} in a nitrogen atmosphere from 25 to 700 °C.

4.3.8. High-Pressure Capillary Rheometer. High-pressure capillary rheological analysis (Rosand RH7D, Malvern Instruments, UK) was utilized to test the shear flow behavior of different composition materials. The experimental parameters were set as follows: L/D = 20/2180 °C and a shear rate range of 50−1500 s^{-1}.

4.3.9. Torque Rheometer. A torque rheometer (Rm-200c, Harbin Hapro Electric Technology Co., Ltd., China) was utilized to test the torque rheological properties of materials with different compositions. About 50 g of the sample was added to the rheometer to melt and mix at 180 °C, and the motor speed was set at 50 rpm/min for 10 min. During the experiment, the torque curve was recorded by the computer.

4.3.10. Mechanical Properties. The universal tensile testing machine (M-4010, Regal Instruments Co., Ltd., China) was utilized to test the tensile strength and elongation at break. The experimental samples were subjected to conventional tensile tests according to the test standard ASTM D412, with a tensile speed of 50 mm/min.

AUTHOR INFORMATION

Corresponding Author

Shibing Bai − *State Key Laboratory of Polymer Materials Engineering, Polymer Research Institute of Sichuan University, Chengdu 610065, China;* orcid.org/0000-0001-8798-8768; Email: baishibing@scu.edu.cn

https://doi.org/10.1021/acsomega.1c06825
ACS Omega 2022, 7, 19113−19121

Authors

Yi Liao − *State Key Laboratory of Polymer Materials Engineering, Polymer Research Institute of Sichuan University, Chengdu 610065, China*

Shuangxin Lai − *State Key Laboratory of Polymer Materials Engineering, Polymer Research Institute of Sichuan University, Chengdu 610065, China*

Shuangqiao Yang − *State Key Laboratory of Polymer Materials Engineering, Polymer Research Institute of Sichuan University, Chengdu 610065, China*

Jinjing Liu − *State Key Laboratory of Special Functional Waterproof Materials, Beijing Oriental Yuhong Waterproof Technology Co., Ltd., Beijing 100020, Peoples' Republic of China*

Adrian L. Kelly − *Centre for Pharmaceutical Engineering Science and IRC in Polymer Engineering, University of Bradford, Bradford BD7 1DP, U.K.*

Complete contact information is available at: https://pubs.acs.org/10.1021/acsomega.1c06825

Notes

The authors declare no competing financial interest.

■ ACKNOWLEDGMENTS

This work was supported by the National Key Research and Development Project (no. 2019YFC1908205) and Funds for International Cooperation and Exchange of the National Natural Science Foundation of China (no. 51861165203) and the Program for Featured Directions of Engineering Multi-disciplines of Sichuan University (no. 2020SCUNG203).

■ REFERENCES

(1) Kato, T.; Onozawa, R.; Miyake, H.; Tanaka, Y.; Takada, T. Properties of Space Charge Distributions and Conduction Current in XLPE and LDPE under DC High Electric Field. *Electr. Eng. Jpn.* **2017**, *198*, 19−26.

(2) Chang, B. P.; Akil, H. M.; Nasir, R. B. M.; Bandara, I. M. C. C. D.; Rajapakse, S. The effect of ZnO nanoparticles on the mechanical, tribological and antibacterial properties of ultra-high molecular weight polyethylene. *J. Reinf. Plast. Comp.* **2014**, *33*, 674−686.

(3) Tone, S.; Hasegawa, M.; Pezzotti, G.; Puppulin, L.; Sudo, A. Effect of e-beam sterilization on the in vivo performance of conventional UHMWPE tibial plates for total knee arthroplasty. *Acta Biomater.* **2017**, *55*, 455−465.

(4) Roettger, M.; Domenech, T.; van der Weegen, R.; Nicolay, A. B. R.; Leibler, L. High-performance vitrimers from commodity thermoplastics through dioxaborolane metathesis. *Science* **2017**, *356*, 62−65.

(5) Al-Malaika, S.; Riasat, S.; Lewucha, C. Reactive antioxidants for peroxide crosslinked polyethylene. *Polym. Degrad. Stab.* **2017**, *145*, 11−24.

(6) Niu, Y. H.; Liang, W. B.; Zhang, Y. L.; Chen, X. L.; Lai, S. Y.; Li, G. X.; Wang, D. J. Crosslinking kinetics of polyethylene with small amount of peroxide and its influence on the subsequent crystallization behaviors. *Chin. J. Polym. Sci.* **2016**, *34*, 1117−1128.

(7) Haussler, M.; Eck, M.; Rothauer, D.; Mecking, S. Closed-loop recycling of polyethylene-like materials. *Nature* **2021**, *590*, 423−427.

(8) Singh, N.; Hui, D.; Singh, R.; Ahuja, I. P. S.; Feo, L.; Fraternali, F. Recycling of plastic solid waste: A state of art review and future applications. *Compos. Part B* **2017**, *115*, 409−422.

(9) Han, S.; Bang, J.; Choi, D. H.; Hwang, J.; Kim, T.; Oh, Y.; Hwang, Y.; Choi, J.; Hong, J. Surface Pattern Analysis of Microplastics and Their Impact on Human-Derived Cells. *ACS Appl. Polym. Mater.* **2020**, *2*, 4541−4550.

(10) Goto, T.; Ashihara, S.; Kato, M.; Okajima, I.; Sako, T. Use of Single-Screw Extruder for Continuous Silane Cross-Linked Polyethylene Recycling Process Using Supercritical Alcohol. *Ind. Eng. Chem. Res.* **2012**, *51*, 6967−6971.

(11) Goto, T.; Ashihara, S.; Yamazaki, T.; Okajima, I.; Sako, T.; Iwamoto, Y.; Ishibashi, M.; Sugeta, T. Continuous Process for Recycling Silane Cross-Linked Polyethylene Using Supercritical Alcohol and Extruders. *Ind. Eng. Chem. Res.* **2011**, *50*, 5661−5666.

(12) Feng, X.; Li, Q.; Wang, K. Waste Plastic Triboelectric Nanogenerators Using Recycled Plastic Bags for Power Generation. *ACS Appl. Mater. Interfaces* **2021**, *13*, 400−410.

(13) Faraj, R. H.; Ali, H. F. H.; Sherwani, A. F. H.; Hassan, B. R.; Karim, H. Use of recycled plastic in self-compacting concrete: A comprehensive review on fresh and mechanical properties. *J. Build Eng.* **2020**, *30*, 101283.

(14) Backstrorn, E.; Odelius, K.; Hakkarainen, M. Designed from Recycled: Turning Polyethylene Waste to Covalently Attached Polylactide Plasticizers. *ACS Sustainable Chem. Eng.* **2019**, *7*, 11004−11013.

(15) Al-Salem, S. M.; Antelava, A.; Constantinou, A.; Manos, G.; Dutta, A. A review on thermal and catalytic pyrolysis of plastic solid waste (PSW). *J. Environ. Manage.* **2017**, *197*, 177−198.

(16) Kumagai, S.; Yoshioka, T. Feedstock Recycling via Waste Plastic Pyrolysis. *J. Jpn. Petrol Inst.* **2016**, *59*, 243−253.

(17) Zhang, X. S.; Lei, H. W.; Chen, S. L.; Wu, J. Catalytic co-pyrolysis of lignocellulosic biomass with polymers: a critical review. *Green Chem.* **2016**, *18*, 4145−4169.

(18) He, P.; Bai, S. B.; Wang, Q. Structure and performance of Poly(vinyl alcohol)/wood powder composite prepared by thermal processing and solid state shear milling technology. *Compos., Part B* **2016**, *99*, 373−380.

(19) Yang, S. Q.; Bai, S. B.; Wang, Q. Morphology, mechanical and thermal oxidative aging properties of HDPE composites reinforced by nonmetals recycled from waste printed circuit boards. *Waste Manage.* **2016**, *57*, 168−175.

(20) Sun, F. S.; Yang, S. Q.; Wang, Q. Selective Decomposition Process and Mechanism of Si-O-Si Cross-Linking Bonds in Silane Cross-Linked Polyethylene by Solid-State Shear Milling. *Ind. Eng. Chem. Res.* **2020**, *59*, 12896−12905.

(21) Yang, S. Q.; Bai, S. B.; Wang, Q. Preparation of fine fiberglass-resin powders from waste printed circuit boards by different milling methods for reinforcing polypropylene composites. *J. Appl. Polym. Sci.* **2015**, *132*, DOI: 10.1002/app.42494.

(22) Sirisinha, K.; Meksawat, D. Comparison in processability and mechanical and thermal properties of ethylene-octene copolymer crosslinked by different techniques. *J. Appl. Polym. Sci.* **2004**, *93*, 1179−1185.

(23) Sun, F.; Bai, S.; Wang, Q. Structures and properties of waste silicone cross-linked polyethylene de-cross-linked selectively by solid-state shear mechanochemical technology. *J. Vinyl Addit. Technol.* **2018**, *25*, 149−158.

(24) Li, D. D.; Greenfield, M. L. Chemical compositions of improved model asphalt systems for molecular simulations. *Fuel* **2014**, *115*, 347−356.

(25) Sun, F.; Yang, S.; Bai, S.; Wang, Q. Reuse of Pan-milled P-XLPE cable powder as additive for asphalt to improve thermal stability and decrease processing viscosity. *Constr. Build. Mater.* **2021**, *281*, 122593.

(26) Silverstein, R. M.; Rodin, J. O. Spectrometric Identification of Organic Compounds on a Milligram Scale - Use of Complementary Information. *Microchem. J.* **1965**, *9*, 301.

(27) Bagus, P. S.; Ilton, E. S.; Nelin, C. J. The interpretation of XPS spectra: Insights into materials properties. *Surf. Sci. Rep.* **2013**, *68*, 273−304.

(28) Wu, H. J.; Liang, M.; Lu, C. H. Morphological and Structural Development of Recycled Crosslinked Polyethylene During Solid-State Mechanochemical Milling. *J. Appl. Polym. Sci.* **2011**, *122*, 257−264.

(29) Yang, S. Q.; Bai, S. B.; Duan, W. F.; Wang, Q. Production of Value-Added Composites from Aluminum-Plastic Package Waste via

Solid-State Shear Milling Process. *ACS Sustainable Chem. Eng.* **2018**, *6*, 4282−4293.
(30) Liu, B. H.; Li, Y. J.; Wang, Q.; Bai, S. B. Green fabrication of leather solid waste/thermoplastic polyurethanes composite: Physically de-bundling effect of solid-state shear milling on collagen bundles. *Compos. Sci. Technol.* **2019**, *181*, 107674.
(31) Wei, P. F.; Bai, S. B. Fabrication of a high-density polyethylene/graphene composite with high exfoliation and high mechanical performance via solid-state shear milling. *RSC Adv.* **2015**, *5*, 93697−93705.
(32) Wang, P.; Zhai, F.; Dong, Z. J.; Wang, L. Z.; Liao, J. P.; Li, G. R. Micromorphology of Asphalt Modified by Polymer and Carbon Nanotubes through Molecular Dynamics Simulation and Experiments: Role of Strengthened Interfacial Interactions. *Energy Fuel* **2018**, *32*, 1179−1187.
(33) Xu, T.; Huang, X. M. Study on combustion mechanism of asphalt binder by using TG-FTIR technique. *Fuel* **2010**, *89*, 2185−2190.
(34) Ding, Z.; Li, J.; Zhang, B.; Luo, Y. Rapid and high-concentration exfoliation of montmorillonite into high-quality and mono-layered nanosheets. *Nanoscale* **2020**, *12*, 17083−17092.
(35) Huang, X.; Zhao, Y.-P. Characterization of pore structure, gas adsorption, and spontaneous imbibition in shale gas reservoirs. *J Pet Sci Eng* **2017**, *159*, 197−204.
(36) Shieh, Y. T.; Chuang, H. C. DSC and DMA studies on silane-grafted and water-crosslinked LDPE/LLDPE blends. *J. Appl. Polym. Sci.* **2001**, *81*, 1808−1816.
(37) Chambers, R. C.; Jones, W. E.; Haruvy, Y.; Webber, S. E.; Fox, M. A. Influence of Steric Effects on the Kinetics of Ethyltrimethoxysilane Hydrolysis in a Fast Sol-Gel System. *Chem. Mater.* **1993**, *5*, 1481−1486.
(38) Lu, X.; Isacsson, U. Compatibility and storage stability of styrene-butadiene-styrene copolymer modified bitumens. *Mater. Struct.* **1997**, *30*, 618−626.
(39) Lu, X. H.; Isacsson, U. Laboratory study on the low temperature physical hardening of conventional and polymer modified bitumens. *Constr. Build. Mater.* **2000**, *14*, 79−88.
(40) Vollmer, I.; Jenks, M. J. F.; Roelands, M. C. P.; White, R. J.; van Harmelen, T.; de Wild, P.; van der Laan, G. P.; Meirer, F.; Keurentjes, J. T. F.; Weckhuysen, B. M. Beyond Mechanical Recycling: Giving New Life to Plastic Waste. *Angew. Chem., Int. Ed.* **2020**, *59*, 15402−15423.
(41) Rahman, M.; Brazel, C. S. The plasticizer market: an assessment of traditional plasticizers and research trends to meet new challenges. *Prog. Polym. Sci.* **2004**, *29*, 1223−1248.
(42) Vaughan, A. S.; Swingler, S. G. Thermal-Analysis of Polymeric Sheathing Materials for Fiber Optic Communication Cables. *IEEE Conf. Publ.* **1993**, *363*, 57−60.
(43) Zuo, M.; Zheng, Q. Correlation between rheological behavior and structure of multi-component polymer systems. *Sci. Chin. Ser., B* **2008**, *51*, 1−12.
(44) Arrigo, R.; Malucelli, G. Rheological Behavior of Polymer/Carbon Nanotube Composites: An Overview. *Materials* **2020**, *13*, 2771.
(45) Yn-hwang, L. *Molecular theory of polymer viscoelasticity - nonlinear relaxation modulus of entangled polymers*; World Scientific, 2011, 242−256.
(46) Yu, W.; Wu, Z. G.; Zhou, C. X.; Zhao, D. L. Linear viscoelasticity calculation of exfoliated polymer/layer silicate nanocomposites. *Chem. J. Chin. Univ.* **2003**, *24*, 715−718.
(47) Kubo, K.; Masamoto, J. Application of elastomer-toughened poly(phenylene sulfide) to gasohol material. *Kobunshi Ronbunshu* **2002**, *59*, 88−92.
(48) Zhang, X.; Yang, H.; Song, Y.; Zheng, Q. Influence of crosslinking on crystallization, rheological, and mechanical behaviors of high density polyethylene/ethylene-vinyl acetate copolymer blends. *Polym. Eng. Sci.* **2014**, *54*, 2848−2858.

https://doi.org/10.1021/acsomega.1c06825
ACS Omega 2022, 7, 19113−19121